J Solid State Electrochem (2008) 12:1325–1336
DOI 10.1007/s10008-008-0539-x

ORIGINAL PAPER

Insights into the electro-oxidation of hydrazine at single-walled carbon-nanotube-modified edge-plane pyrolytic graphite electrodes electro-decorated with metal and metal oxide films

Abolanle S. Adekunle · Kenneth I. Ozoemena

Received: 8 December 2007 / Accepted: 28 February 2008 / Published online: 2 April 2008

Abstract Electrochemistry of edge-plane pyrolytic graphite electrodes (EPPGEs) modified with Aldrich single-walled carbon nanotubes (SWCNTs) electro-decorated with metal (Ni, Fe and Co) and their oxides have been studied. The morphology and identity of the metallic dispersions were examined by scanning electron microscopy and energy-dispersive spectroscopy. We show that SWCNTs serve as efficient conducting carbon material for electronic communication between metal films and the underlying carbon electrode. By using cyclic voltammetry and electrochemical impedance spectroscopy (EIS) techniques, it is proved that both EPPGE-SWCNT-Ni and EPPGE-SWCNT-Fe exhibit comparable electrochemical response in buffered aqueous solution (pH 7.0) and towards electro-oxidation of hydrazine in Na_2SO_4 solution. The impedance spectra of these SWCNT-metal hybrids were complicated and follow electrical equivalent circuit model typical of adsorption-controlled charge transfer kinetics. Hydrazine impedance spectra exhibited inductive loop, characteristic of Faradaic current being governed by the occupation of an intermediate state. On the other hand, the EIS data obtained in a simple redox probe, $[Fe(CN)_6]^{3-}/[Fe(CN)_6]^{4-}$, showed that EPPGE-SWCNT and EPPGE-SWCNT-Ni followed electrical equivalent circuit models typical of partial charge transfer or adsorption-controlled kinetics with some resemblance to the behaviour of electrolyte–insulator–semiconductor sensors.

Keywords Single-walled carbon nanotubes · Metal and metal oxide films · Electro-oxidation of hydrazine · Cyclic voltammetry · Electrochemical impedance spectroscopy

A. S. Adekunle · K. I. Ozoemena (✉)
Department of Chemistry, University of Pretoria,
Pretoria 0002, South Africa
e-mail: kenneth.ozoemena@up.ac.za

Introduction

Electro-oxidation of hydrazine (N_2H_4) on carbon surfaces has continued to receive significant research interests [1–16] due to the extensive applications of hydrazine and its derivatives in a plethora of areas relating to chemical industry, military, agriculture and pharmaceuticals. Hydrazine is regarded as an important anodic material for fuel cell and used for zero-emission fuel cells and used as a fuel in high-energy propellant in rockets and spacecrafts by the military and aerospace industries [6, 15, 16]. On the negative side, hydrazine and its methyl derivatives have been implicated as potential carcinogens and mutagens and hepatotoxic substances that could cause liver and kidney damages have also been reported and well established [17]. Also, in 2003, hydrazine was implicated in a terrorist incident [18]. It could be said therefore that it is this dual purpose of hydrazine as useful materials in several applications such as fuel cell development and as hazardous substances that underpins the need to investigate its electro-oxidative behaviour at low cost and easily available carbon electrodes.

Carbon electrodes (such as the glassy carbon, carbon paste, highly oriented pyrolytic graphites, basal plane and edge-plane pyrolytic graphites) have long been recognised as versatile and supporting platforms for electrocatalysis and electrochemical sensing due to their numerous advantages (such as low cost, chemical inertness and wide potential window in most electrolyte solutions) over the precious metal electrodes. Carbon nanotubes, discovered in 1978 [19] and rediscovered in 1991 [20], occur in two main types: single-walled carbon nanotubes (SWCNTs) which consist of single rolled-up graphite sheet or single graphite tube and multi-walled carbon nanotubes (MWCNTs), which consist of several sheets of graphites rolled into

concentric tubes. Carbon-nanotube-based electrodes have been receiving considerable attention in electrochemistry because of their intriguing ability to enhance the electrochemical responses of several molecules of industrial, environmental and biomedical importance [21–35]. Research reports have continued to suggest that smart decoration of carbon nanotubes with metal nanoparticles [36–45] of desired optical, magnetic, electrical and catalytic properties could be harnessed for the development of numerous potential applications ranging from high-performance nanoscale devices, nanoelectronics through advanced electrocatalytic systems and sensors to highly efficient fuel cells.

Despite the huge literature on the electro-oxidation of hydrazine on carbon-based electrodes [1–10, 46–56], the use of carbon nanotubes decorated with metal nanoparticle is limited [49]. Hitherto, all attention on CNT-supported metal nanoparticles, as evident in the recent review by Wildgoose et al. [45], has been directly only on metals such as Pt, Pd, Ru, Ag and Au. It has also been constantly reported that HiPCo MWCNTs and SWCNTs are inherently contaminated with iron nanoparticles explaining why "electrocatalysis" observed on such CNT-based carbon electrodes [57–63] for certain analytes, including hydrazine [58], are or could be strongly influenced by the iron nanoparticle impurities. Our group [63] has recently shown that the main impurities in the Aldrich SWCNTs are nickel particles but these metallic impurities did neither show any detectable impact on the SWCNTs electron transfer kinetics of $[Fe(CN)_6]^{3-}/([Fe(CN)_6]^{4-})$ nor influence the electrochemical response of the degradation products of V-type nerve agents. More recently, however, Kruusma et al. [58] demonstrated that HiPCo SWCNTs contain residual iron oxide impurities which dominated their electrochemical activity towards the detection of hydrogen peroxide and hydrazine. We suspect that the differences in these reports could point to differences in analytes being investigated. Given the ability of iron impurities in CNTs to influence electro-oxidation of hydrazine [58], it could be interesting to explore the electrochemical response of metal-decorated SWCNTs ('deliberate metal impurification') towards the electro-oxidation of hydrazine. To the best of our knowledge, no consideration has been given to this type of investigation, especially with nickel and iron nanoparticles which have been established to be the major contaminants of SWCNTs.

Thus, in this communication, we explore the electro-oxidation of hydrazine at edge-plane pyrolytic graphite electrode pre-modified with acid-treated and washed SWCNTs and then electro-decorated with metal (Fe, Ni and Co) nanoparticles and their oxides. For the first time, we show that SWCNT-nickel system, much like its SWCNT-iron hybrid counterpart, enhances the response of the electro-oxidation of hydrazine. We also established that these SWCNT-metal hybrids exhibit complicated electrochemical impedance spectra, compatible only with electrical equivalent circuit model characteristic of adsorption-controlled charge transfer kinetics.

Experimental

The SWCNTs (06509HB Aldrich) was purchased from Aldrich and digested by subjecting it to harsh acid conditions for –COOH modification following the method already described [33, 44, 64–69]. The nitrate salts of the metals, $Ni(NO_3)_2{\cdot}6H_2O$, $Fe(NO_3){\cdot}9H_2O$, $Co(NO_3)_2{\cdot}6H_2O$, the hydrazine sulphate, sodium sulphate and other reagent were of analytical grade. Ultra-pure water with resistivity of 18.2 MΩ was obtained from a Milli-Q Water System (Millipore Corp., Bedford, MA, USA) and was used throughout for the preparation of solutions. All electrochemical experiments were performed with nitrogen-saturated buffer solutions. All other reagents were of analytical grades and were used as received from the suppliers without further purification. Acetate and phosphate buffer solutions (0.1 M) of pH 4.0 and 7.0, respectively, were prepared using CH_3COOH, CH_3COONa, $NaH_2PO_4.2H_20$ and $Na_2HPO_4.2H_2O$. All solutions were prepared using double-distilled deionised water and purged with pure nitrogen to eliminate oxygen and any form of oxidation during experiment.

The edge-plane pyrolytic graphite electrode plate (4-mm diametre) was purchased from Le Carbone, Sussex, UK and was constructed in-house at the University of Pretoria technical workshop by placing it in a Teflon tube, extended outside with a copper wire to make electrical contact with the electrochemical equipment as already described in the literature [34, 35, 62, 63]. Field emission scanning electron microscopy (FESEM) images were obtained from JEOL JSM 5800 LV (Japan) while the energy-dispersive X-ray spectra were obtained from NORAN VANTAGE (USA) at the Microscopy and Microanalysis Laboratory of the University of Pretoria. Electrochemical experiments were carried out using an Autolab Potentiostat PGSTAT 302 (Eco Chemie, Utrecht, The Netherlands) driven by the General Purpose Electrochemical System software version 4.9. Electrochemical impedance spectroscopy (EIS) measurements were performed with an Autolab Frequency Response Analyser software between 10 Hz and 100 kHz using a 5-mV rms sinusoidal modulation. A Ag|AgCl in saturated KCl and platinum wire were used as reference and counter electrodes, respectively. A bench top pH/ISE ORION metre, model 420A, was used for pH measurements. All solutions were de-aerated by bubbling nitrogen prior to each electrochemical experiment. All experiments were performed at 25±1 °C.

Electrodes were prepared using the following procedures. First, the edge-plane pyrolytic graphite electrodes (EPPGE) surface was cleaned by gentle polishing in aqueous slurry of alumina oxide nanopowder (Sigma-Aldrich) on a SiC-emery paper and then to a mirror finish on a Buehler felt pad. The electrode was then subjected to ultrasonic vibration in acetone to remove residual alumina particles that might be trapped at the surface. EPPGE-SWCNT was prepared by drop-dry method. About 20-μL drop of the SWCNTs-dimethylformamide (DMF) solution (7-mg acidified SWCNTs in 1 ml DMF) was dropped on the bare EPPGE and dried in an oven at 50 °C for about 2 min. The EPPGE-SWCNT-M (where M = Fe or Ni or Co) was obtained using similar procedure adopted by others [33, 44, 64–66, 69] for the electrodeposition of metal nanoparticles on carbon electrodes using chrono-amperometric strategy. Briefly, EPPGE-SWCNT was immersed in 5-mM solution of the nitrate salts of the metals, $(Ni(NO_3)_2{\cdot}6H_2O$ or $Fe(NO_3){\cdot}9H_2O)$ or $Co(NO_3)_2{\cdot}6H_2O$, at a fixed potential of −2.0 V (vs Ag|AgCl, sat'd KCl) for 5 min. We chose 5-min deposition time as reported by Salimi et al. [33, 64–66]. Also, preliminary investigation of electrochemical response of EPPGE-SWCNT-Ni in 0.1-M NaOH solution obtained at different deposition times intervals of between 5 and 40 min (not shown here) yielded the lowest surface coverage of nickel and least current response. The electrodes, EPPGE-SWCNT-MO (where M = Fe, Ni or Co) were obtained by immersing the EPPGE-SWCNT-M in 0.1 M phosphate-buffered saline (pH 7.0) and repetitively scanning (20 scans) between 1.5 and −0.8-V potential window at a scan rate of 100 mV/s. The electroactive areas of the electrodes were estimated from the conventional Randle Sevcik equation using the electrochemistry of $[Fe(CN)_6]^{4-}/[Fe(CN)_6]^{3-}$ [70] to be approximately 0.13 cm^2. Procedure for the electro-oxidation of hydrazine was adopted from previous works [1–16, 71].

Results and discussion

Comparative FESEM images and electron-dispersive X-rays

Figure 1 compares the scanning electron microscopy (SEM) images of the bare EPPGE, EPPGE-SWCNT and EPPGE-SWCNT-Ni. The edge-plane sites of the EPPGE are evident in its SEM image (Fig. 1a).

Upon modification of the EPPGE with the acid-treated and washed SWCNTs, the morphology shows aggregated

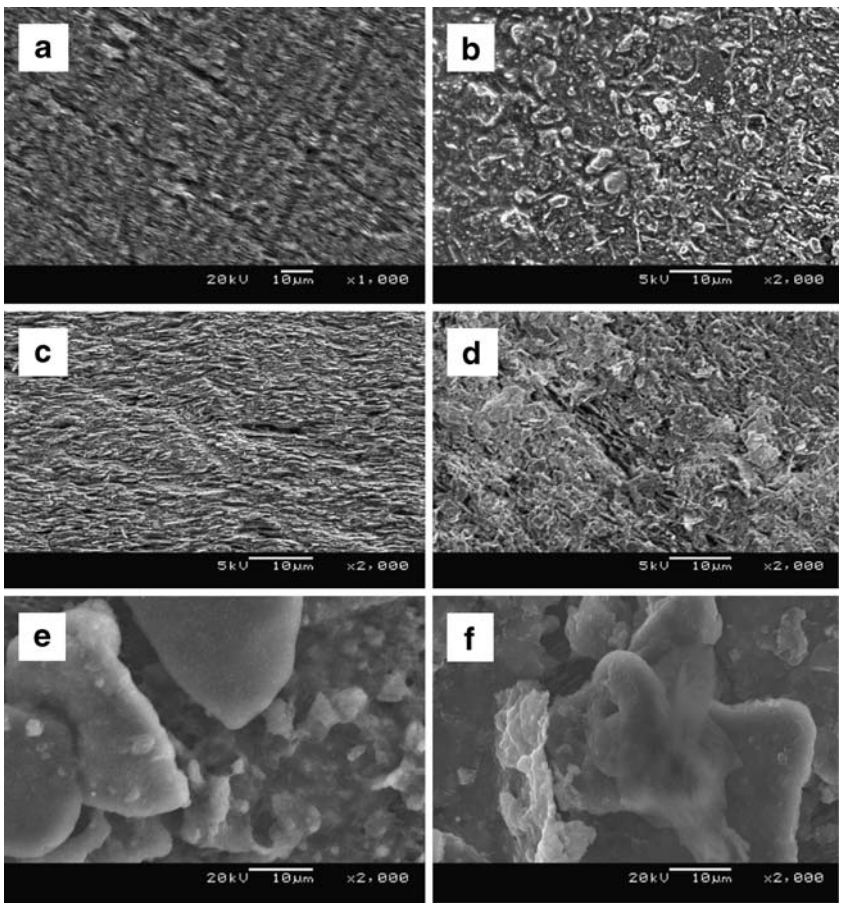

Fig. 1 Typical FESEM images of the **a** bare EPPGE, **b** EPPGE-SWCNT, **c** EPPGE-SWCNT-Ni, **d** EPPGE-SWCNT-Fe, **d** EPPGE-SWCNT-NiO and **f** EPPGE-SWCNT-FeO

SWCNTs (Fig. 1b). Upon introduction of the metal particles, we observe an interconnected layer-structured network image of the SWCNT-modified EPPGE (Fig. 1c, d). However, upon electrochemical treatment in aqueous solution, these layer-structured networks become disconnected transforming into lumps with exposed interiors (Fig. 1e, f), with sizes in the micrometre ranges. As also speculated by other workers [58, 61], it may be reasonable to assume here that these metal particles could either be trapped in the graphite layers and/or located on the outside of the tubes exposed to the solutions, and/or mixed amongst the aggregated bundles of the tubes. To corroborate the SEM results, energy-dispersive X-ray spectroscopy (EDX) experiments were run at the various electrodes. The EDX profile (Fig. 2) gives the analytical details of the elemental composition of the different electrodes. As expected, the unmodified EPPGE (A) predominantly showed carbon. The acid-treated SWCNT (B) confirmed presence of oxo-functionalities, with sulphur peak which could have arisen from the sulphuric acid solution used in the functionalisation and washing of the SWCNTs.

Traces of nickel impurities on the acid-treated and washed SWCNTs indicate these metal impurities are intrinsic to the Aldrich SWCNTs used in this study and cannot be completely removed. A similar result has recently been reported by Jurkschat et al. [60] for HiPCo SWCNTs and was found to contain iron impurities. The EDX profile of EPPGE-SWCNT-Ni (C) and EPPGE-SWCNT-NiO (D) showed well-defined nickel peaks, confirming the successful electro-decoration of the EPPGE-confined SWCNTs. The occurrence of P and Na peaks in the EDX of EPPGE-SWCNT-NiO is ascribed to the treatment of the electrode with sodium phosphate buffer solution while the enhanced oxygen peak confirms the modification of the electrode to its oxide form. Similar trend in the SEM images and EDX profiles were observed for the Fe- and Co-based electrodes (not shown).

Comparative redox chemistry of modified EPPGEs in aqueous solution

Figure 3 shows examples of the voltammetric responses of the bare and modified EPPGEs (EPPGE-NiO, EPPGE-SWCNT, EPPGE-SWCNT-NiO, EPPGE-SWCNT-FeO and EPPGE-SWCNT-CoO) in 0.1-M phosphate-buffered solution (pH 7.0). We observed successful integration of the metals and metal oxides films with the SWCNTs, confirmed by features such as (1) the presence of the well-defined redox waves of the M(II)/M(III) (M = Ni, Fe and

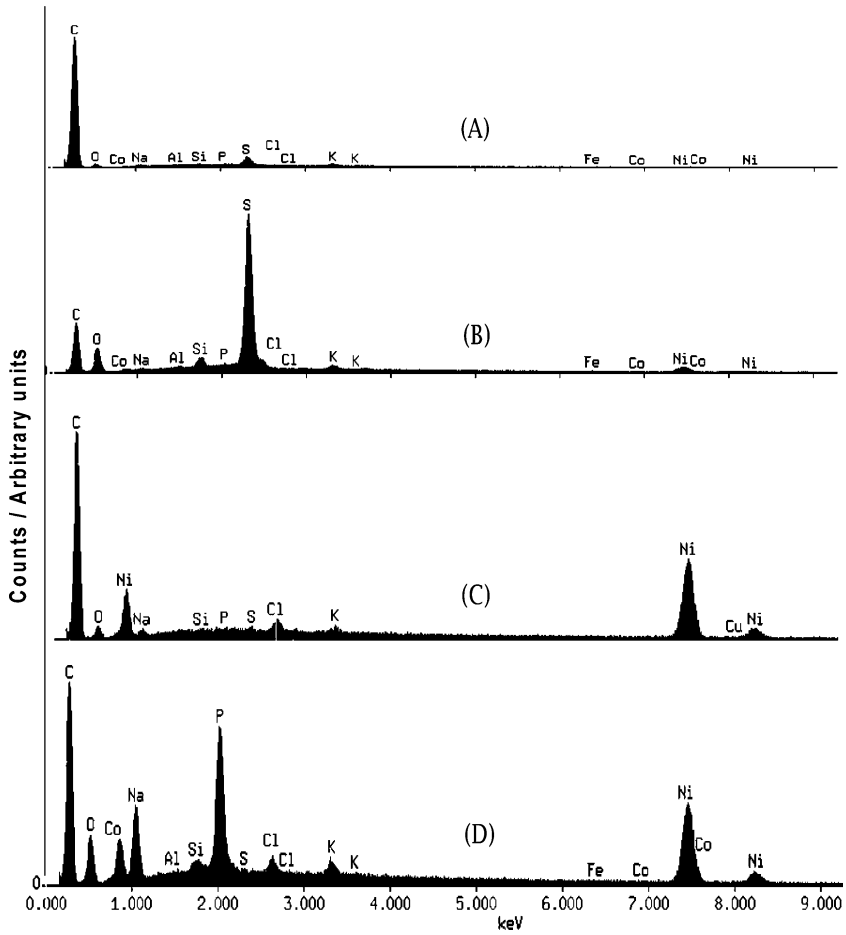

Fig. 2 Typical EDX plots of the (*A*) bare EPPGE, (*B*) EPPGE- SWCNT, (*C*) EPPGE-SWCNT-Ni, and (*D*) EPPGE-SWCNT-NiO

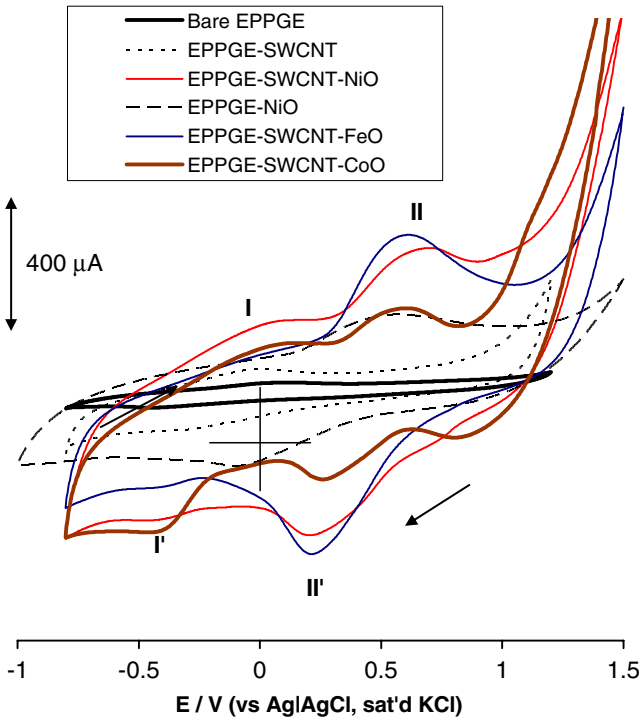

Fig. 3 Examples of voltammetric evolutions of the bare EPPGE and modified EPPGEs in 0.1 M pH 7.0 PBS. Scan rate=50 mV/s. The voltammograms of the modified EPPGEs were obtained after 20 continuous scans. Other scans have been omitted for clarity

Co; $E_{1/2}$≈0.45 V vs Ag|AgCl, sat'd KCl), (2) the increased current response following the incorporation of the metal particles with the SWCNTs and (3) the high background current of the EPPGE-SWCNT-MO compared to other electrodes. These metal oxide nanoparticles exhibit electrochemical stability as the redox peak (II) remained essentially the same even after 50th scan. Some other important features in Fig. 3 are (1) EPPGE-SWCNT exhibited a pair of weak redox peak (E_a≈−0.01 V and E_c≈−0.30 V), which is typical of immobilised SWCNTs at a carbon electrode. The origins of the broad cathodic couples (I/I') are the redox processes of the SWCNTs and/or overlapped processes of the M(I)/M(II) and SWCNTs, while the other couple (II/II') are due to the redox processes of the M(II)/M(III). The voltammograms are unsymmetrical with the ratios of the oxidation to reduction charges larger than unity, which are characteristic of quasi-reversible behaviour [70].

An interesting observation here is the significant decrease in the peak-to-peak separation potential (ΔE) value of the M(II)/M(III) redox process in the presence of SWCNTs (rE=0.37, 0.42 and 0.50 V for CoO, FeO and NiO, respectively) compared to the absence of SWCNTs (ΔE= 0.70 V). Also, the electrochemical response of the cobalt-based electrode is lower than those of the iron- and nickel-based electrodes. In general, the results suggest the ability of the SWCNTs to serve as efficient conducting carbon materials for electronic communication between the metal nanoparticles and the underlying carbon electrode, EPPGE.

Comparative electrocatalytic oxidation of hydrazine

Figure 4 compares the voltammetric evolutions of the various electrodes in 0.1 M Na_2SO_4 containing 1 mM

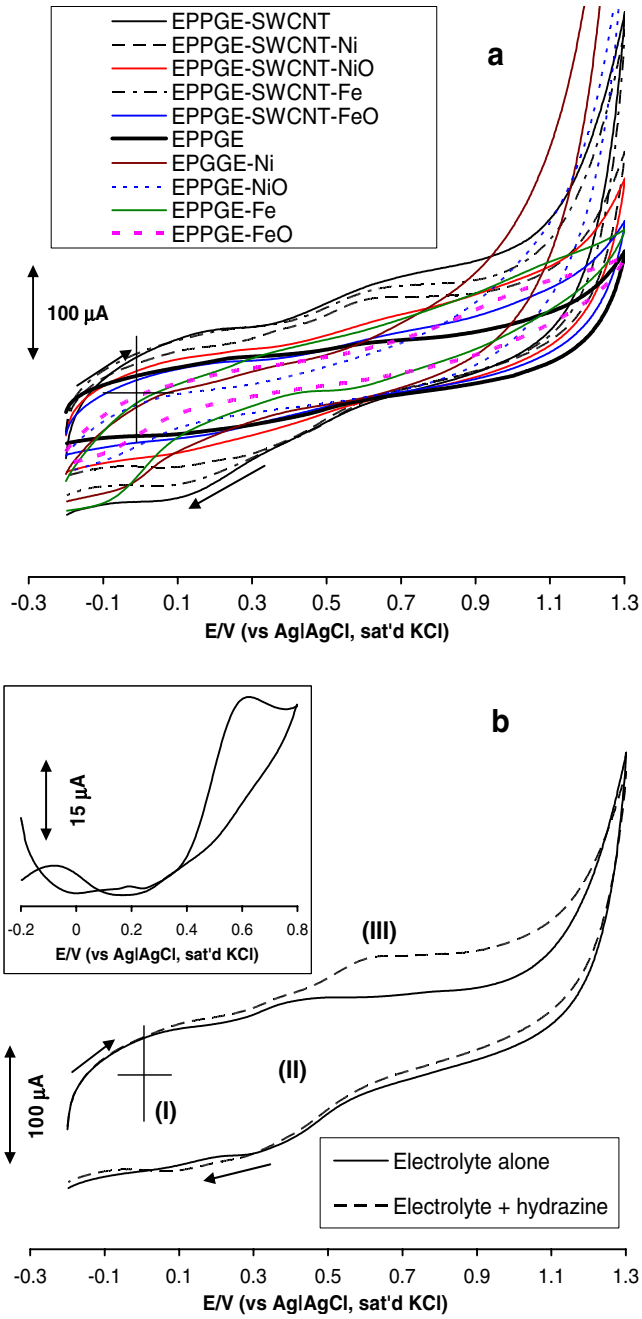

Fig. 4 **a** Examples of cyclic voltammograms recorded at the various electrodes in 0.1-M Na_2SO_4 solution containing 1 mM hydrazine and **b** comparative cyclic voltammograms recorded at the EPPGE-SWCNT-Ni in 0.1 M Na_2SO_4 with and without hydrazine. *Inset* of **b** is the background-subtracted hydrazine response of the EPPGE-SWCNT-Ni. Scan rate=25 mVs^{-1}

hydrazine. For a clearer picture of the electro-oxidative responses of the electrodes, the observed voltammograms were subtracted from those generated by their respective electrolytes (as exemplified in Fig. 4b using the EPPGE-SWCNT-Ni).

Peaks I (broad at ~0.0 V), II ($E_{1/2}$=0.35 V) and III (E_p= 0.60 V) are due to the redox processes of the SWCNTs, nickel and hydrazine oxidation, respectively. In general, peak current of the hydrazine followed this trend: EPPGE-SWCNT-Ni (~ 44 μA) > EPPGE-SWCNT (~ 37 μA) > EPPGE-SWCNT-Fe (~ 26 μA) > EPPGE-SWCNT-CoO (~23 μA) > EPPGE-SWCNT-NiO (~ 21 μA) > EPPGE-SWCNT-Co (~19 μA) > EPPGE-SWCNT-FeO (~ 18 μA) > EPPGE-FeO (~17 μA) > EPPGE-Fe (~ 16 μA) > EPPGE-Ni (~15 μA) ≈ EPPGE-NiO ≈ Bare EPPGE (~ 15 μA). The oxidation peak of the EPPGE-SWCNT-Ni appeared at about 0.6 V while others occurred at slightly more positive potentials (≥ 0.66 V). The bare EPPGE and EPPGE modified with metal and metal oxide layers showed weak electro-oxidative response. The EPPGE modified with metal and metal oxide layers showed weak oxidation peak at more positive potential (*approximately* 0.1 V), suggesting that in the experimental conditions employed in this study, metal and metal oxide layers did not show activity towards hydrazine. The response of the EPPGE-SWCNT is associated with larger background (capacitive) current compared to other electrodes, which is characteristic of acid-treated SWCNTs [72]. The response of SWCNT towards hydrazine oxidation is somewhat controversial. For example, while Guo and Li [47] did not observe any electro-oxidation of hydrazine at SWCNT-paste electrode, Banks and co-workers have consistently observed electro-oxidation of hydrazine at basal plane pyrolytic graphite electrodes modified with either MWCNTs [57, 59] or SWCNTs [58, 60] which they attributed to the presence of iron oxide impurities. Because our EDX results for the Aldrich SWCNTs (B) did not show iron oxide impurities and we did not observe any dramatic current responses with either the EPPGE-SWCNT-Fe or EPPGE-SWCNT-FeO, we can rule out the influence of iron oxide influencing the electro-oxidation of hydrazine; the most likely metal catalyst impurities are the nickel and its oxides. The better electrochemical response exhibited by the EPPGE-SWCNT-Ni compared to other electrodes could be due to the synergistic activities of SWCNTs and Ni particles. The low current response of the metal-oxide-based electrodes is interesting in that, up to now, for example, only carbon electrodes modified with nickel oxide nanoparticles have been reported for electrocatalytic detection. For example, Salimi et al. have used GCEs modified with nickel oxide or cobalt oxide nanoparticles to study the electrochemistry of haemoglobin [33, 64], hydrogen peroxide [44], catalase [65] and glucose oxidase [66]. The low response of the nickel-oxide-modified electrode is attributed to surface layer passivation during electrode modification which results in the layers acting as insulator to charge transfer. Following the better electroactivity of the EPPGE-SWCNT-Ni over the other electrodes, all subsequent studies in this work, unless otherwise stated, were focussed on this electrode.

Electrochemical impedimetric studies

Insights into the electro-oxidation process of hydrazine at these electrodes were obtained from EIS, at a fixed potential (0.6 V vs Ag}AgCl, sat'd KCl). EIS is a powerful non-destructive and very informative technique for probing molecules at surfaces. For example, it provides vital information about the charge transfer phenomenon across the electrode–electrolyte interface [73–78]. Figure 5 shows examples of the impedance spectra (Nyquist plots) obtained with the electrodes, EPPEGE-SWCNT, EPPGE-SWCNT-Fe, EPPGE-SWCNT-Ni and EPPGE-SWCNT-Co at frequencies between 10 kHz and 0.1 Hz.

The impedance spectra were rather complicated, showing small and distorted semi-circle in the high-frequency region. Several efforts to obtain a suitable equivalent circuit, including the original Randles model [58] that describes 'true' Faradaic process (i.e. true charge transfer at the electrode–solution interface) were unsuccessful. However, the equivalent circuit model (Fig. 5b), which incorporates the

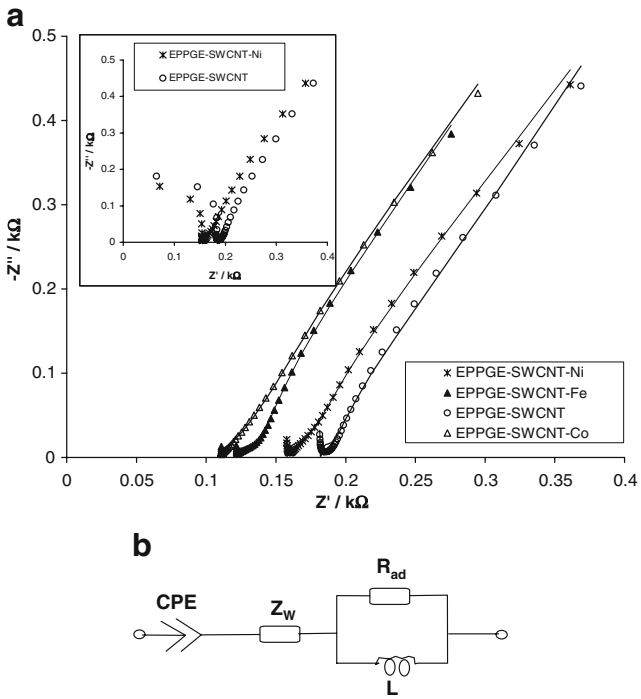

Fig. 5 **a** Examples of typical Nyquist plots of modified EPPGEs obtained in 0.1 M Na_2SO_4 containing 1 mM hydrazine, between 10 kHz and 0.1 Hz. *Inset* are similar plots obtained at 100 kHz and 0.1 Hz. **b** Equivalent circuit model used in fitting the spectra obtained in Fig. 5a

Table 1 Impedance data ($E_{1/2}$=0.6 V) for the electrocatalytic oxidation of 10^{-3} M hydrazine (between 10 kHz and 0.1 Hz) on the modified and unmodified EPPGE electrodes

Electrodes	Q/mF	Number	Z_w/μΩcm^2	L/mHcm^2	R_{ad}/μΩcm^2
EPPGE	0.32 (6.74)	0.62 (3.42)	1.85 (6.34)	0.75 (10.29)	32.60 (3.00)
EPPGE-SWCNT	0.49 (6.29)	0.84 (2.50)	3.92 (5.45)	0.93 (9.27)	45.16 (1.56)
EPPGE-SWCNT-Ni	0.47 (5.25)	0.81 (2.12)	3.67 (5.09)	0.64 (8.59)	32.94 (1.41)
EPPGE-SWCNT-Fe	0.53 (3.95)	0.84 (1.53)	5.34 (4.82)	0.54 (8.04)	31.39 (1.07)
EPPGE-SWCNT-Co	0.50 (4.25)	0.80 (1.67)	5.85 (4.83)	0.50 (7.97)	26.23 (1.32)
EPPGE-SWCNT-NiO	0.37 (4.61)	0.82 (1.79)	2.42 (6.63)	0.39 (9.71)	24.10 (1.36)
EPPGE-SWCNT-FeO	0.28 (3.49)	0.73 (1.33)	8.62 (5.24)	0.41 (8.94)	22.48 (1.71)
EPPGE-SWCNT-CoO	0.35 (4.60)	0.84 (1.67)	3.69 (6.03)	0.36 (9.81)	19.95 (1.47)

NOTE: All values were obtained from the fitted impedance spectra after several iterations using the circuits. Note that the values in parentheses are percent errors of data fitting.

constant phase element (CPE) and an inductor L, yielded satisfactory results as evident from the low percentage error values as evident in Table 1. These EIS data were obtained from fitting the equivalent circuits after several iterations. Presently, the impedance behaviour of the electro-oxidation of hydrazine is virtually non-existent. From the abstract of the only existing report on the electro-oxidation of hydrazine, carried out in alkaline solution on Pd dispersed over graphite cloth, by Duarte et al. [51], it is understood that the impedance behaviour of the system was also complex. The complexity of the spectra was attributed to several factors including electrode structure, interfacial graphite properties and reaction kinetics. The authors [51] also observed small and distorted semi-circle in the high-frequency region which they attributed to the porous structure of this carbon-based electrode. We may also associate the complex impedance behaviour observed in our system to the same factors as interpreted by Duarte et al. [51]. The absence of the solution resistance in the equivalent circuit model suggests that at high frequency the spectra (semi-circle) could possibly extend to the zero point of the real and imaginary impedance plots. Figure 5 (inset) shows Nyquist plots carried out between 100 kHz and 0.1 Hz, indicating the possibility of obtaining such semi-circle loop extending the zero point. In this electrical equivalent circuit (Fig. 5b), R_{ad} (resistance to adsorption) and L are well known as electrical elements associated with the adsorption of reaction intermediate(s) [79–81], clearly suggesting the involvement of the hydrazine intermediate products in the overall electro-oxidative process. Duarte et al. [51] also detected the existence of an adsorbed intermediate in their system. In electrocatalytic reactions, it is known that inductive behaviour takes place when the Faradaic current is governed by the occupation of an intermediate state [79, 81]. The R_{ad} value is therefore interpreted here as the consequence of the adsorption of the intermediate(s) on the electrodes. The R_{ad} values of the metal oxide films are slightly less than those of their metal films, suggesting that the adsorption process is less pronounced at the metal oxides films. CPE is ascribed to the geometrical or energetic inhomogeneity of the surface and it is related to n. The n is a factor describing the deviation from the ideal capacitive behaviour (i.e. n=1.0). Thus, the n value of less than the ideal 1.0 is indicative of pseudo-capacitive processes confirming the presence of the CPE in the circuit. The Warburg (Z_w) impedance relates to the semi-infinite linear diffusion. We attribute this occurrence of the inductance to be due to the electrode, possibly due to the intermediate adsorbed species during the electro-oxidative reactions of hydrazine (further discussed below).

More information on the electrical properties of the electrodes during hydrazine oxidation are provided by closer look at the Bode plot (Fig. 6).

The appearance of a dip or curve in the high-frequency region (Fig. 6) rather than a peak, normally observed for solution resistance (R_s) in the high-frequency region, could indicate the dominance of the inductance phenomenon over the solution resistance. The peak at about −35°

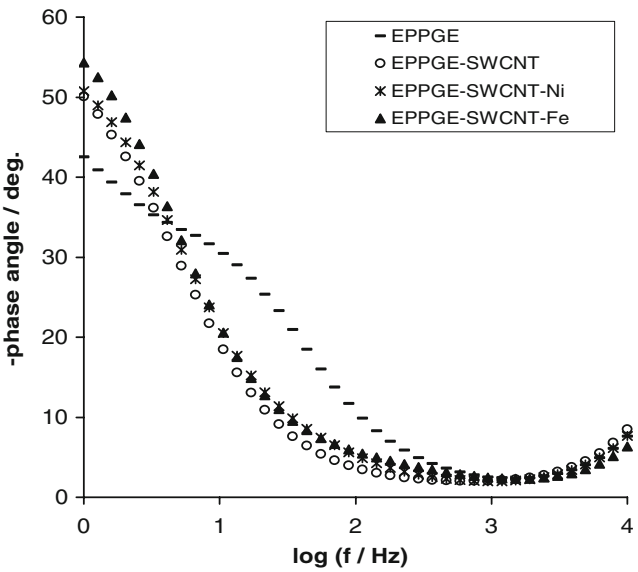

Fig. 6 Examples of typical Bode plots of modified EPPGEs obtained in 0.1 M Na_2SO_4 containing 1 mM hydrazine, between 10 kHz and 0.1 Hz

depicts the relaxation process of the EPPGE–solution interface; the disappearance of this peak confirms the modification of the EPPGE and replacement by the EPPGE-SWCNT-M film–solution interface.

Inductive behaviour at high-frequency range is thought to be due to either the (1) instrumental artifacts, or (2) the inductance of the electrode, or (3) the inductance of the connecting wires (Research Solutions and Resources available online at: http://www.consultrsr.com/resources/eis/induct2.htm). To attempt to rule out (1) and (3), we repeated the experiment more than seven times, but the same results were obtained. To provide some insights into the possibility of the electrode itself, i.e., possibility (3), we thought it was necessary to carry the experiment in a simple redox system. We examined the cyclic voltammetric and impedance spectral evolutions of the EPPGE-SWCNT and EPPGE-SWCNT-Ni in the presence of simple redox probe, $[Fe(CN)_6]^{4-}$/$[Fe(CN)_6]^{3}$. As shown in Fig. 7, the voltammograms showed redox peak at 0.30 V for the EPPGE-SWCNT and broad redox peak at 0.45 V for the EPPGE-SWCNT-Ni. We attribute the broad peak of the EPPGE-SWCNT-Ni to possible overlap of the $[Fe(CN)_6]^{4-}$/$[Fe(CN)_6]^{3-}$ and Ni (II)/Ni(III) redox processes.

Thus, the EIS was performed at 0.3 V for both electrodes and also at 0.45 V for the EPPGE-SWCNT-Ni. The Nyquist plots in Fig. 8 show the experimental data fitted with the equivalent model (Fig. 8b).

It should be clearly seen that, unlike in hydrazine solution, the equivalent circuit model (Fig. 8b) incorporates the R_s (the solution–electrolyte resistance) with no inductive behaviour. The excellent fitting of the theoretical model (Fig. 8b) with our experimental spectra clearly justifies our choice of this circuit model. Interestingly, we notice

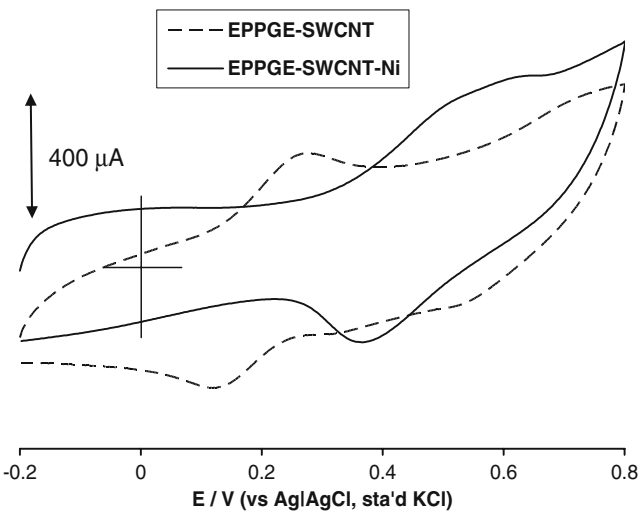

Fig. 7 Typical comparative cyclic voltammetric evolutions of the electrodes (EPPGE-SWCNT and EPPGE-SWCNT-Ni) in 5-mM $[Fe(CN)_6]^{4-}$/$[Fe(CN)_6]^{3-}$ solution (PBS pH 7.0). Scan rate=CVs (50 mV/s)

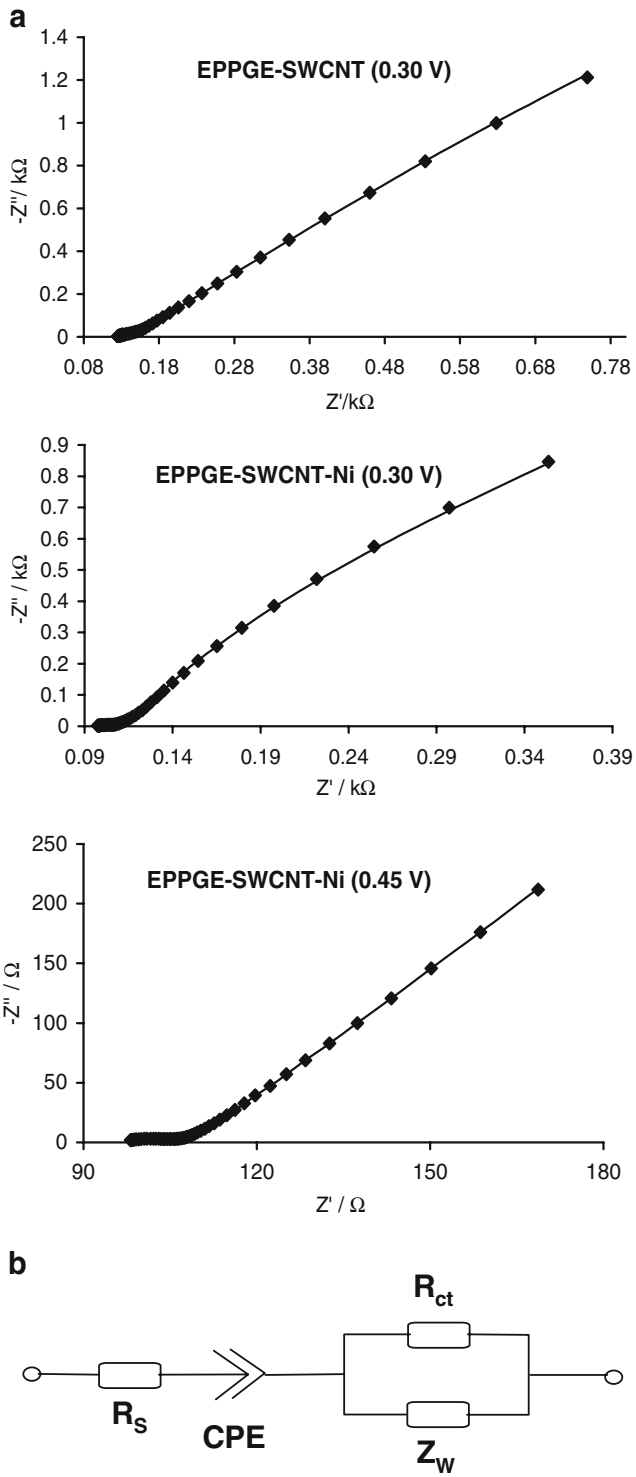

Fig. 8 **a** Typical Nyquist plots of the of the electrodes obtained in 5-mM $[Fe(CN)_6]^{4-}$/$[Fe(CN)_6]^{3-}$ solution (PBS pH 7.0) at fixed potential of 0.30 and 0.45 V vs Ag|AgCl sat'd KCl. The *square* data points are experimental while the *solid lines* in the spectra show non-linear least-squares fits. **b** Equivalent circuit model used in fitting the spectra obtained in Fig. 8

from literature [82] that this equivalent circuit exhibits good resemblance to the equivalent circuit of the "electrolyte–insulator–semiconductor (EIS)" sensors. An electro-

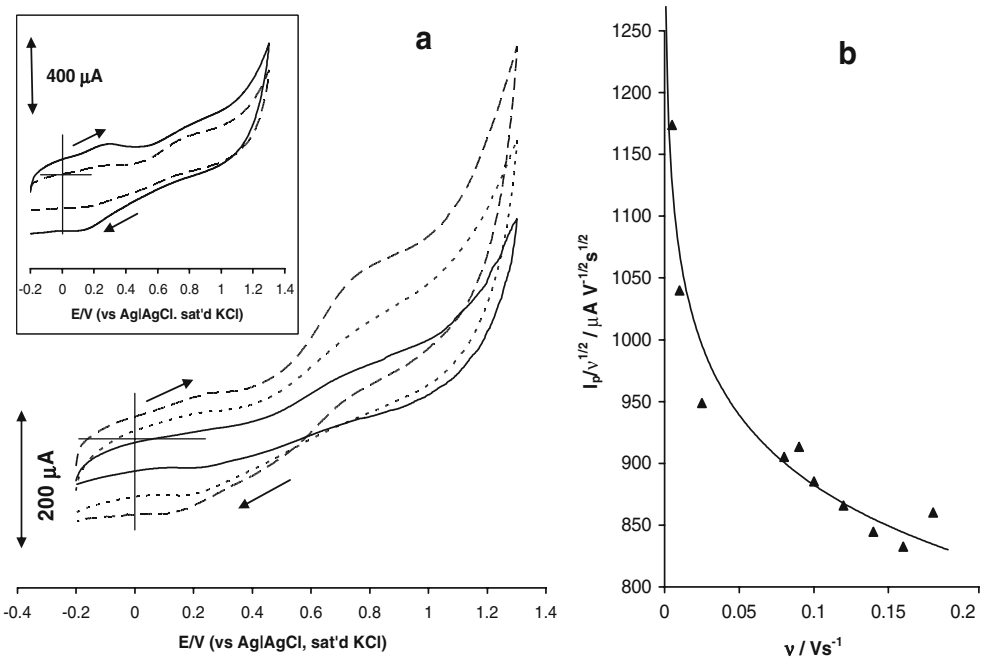

Fig. 9 **a** Examples of cyclic voltammetric evolutions of EPPGE-SWCNT-Ni obtained in 0.1 M Na_2SO_4 containing 1 mM hydrazine at scan rates 10, 25 and 50 mV s^{-1} (inner to outer). Inset compares voltammograms obtained at 50 and 140 mVs^{-1} (inner to outer). **b** Current function plot, $I_p/\nu^{1/2}$ vs ν

lyte–insulator–semiconductor device comprises a doped semiconductor acting as substrate for a thin insulating layer, normally an oxide or nitride, which can be immersed in an electrolyte containing a fixed concentration of anionic species to be measured. Indeed, the most important message here is the distinct difference between the EIS data in hydrazine solution and data from solution of simple redox probe, which clearly indicate that these results are not just the consequences of electrode geometry but electrode mechanisms (notably adsorption phenomena). More detailed study is being undertaken for the EIS evolutions for these electrodes.

Effect of varying scan rates

Cyclic voltammetric experiments were carried out with a view to establishing the impact of scan rates (ν) at constant concentration (0.01 M) of the hydrazine in 0.1 M Na_2SO_4 solution (Fig. 9). We observed that hydrazine peak at 0.6 V and the Ni(II)/Ni(III) redox peak at 0.2 V simultaneously increase with increase in scan rates (scan rates ranging from 10 to 200 mV s^{-1}). At>100 mV s^{-1} (see inset of Fig. 9), the Ni(II)/Ni(III) redox process became more pronounced than the hydrazine peak. We have no firm explanation for this surprising and rare occurrence at this moment, but it may not be unconnected with electrode fouling by intermediate products (radicals) of the hydrazine electro-oxidation (due to adsorption) coupled with the efficient reductive activity of hydrazine solution towards nickel ions as reported by the Bettahar group [83, 84].

The plot of peak current versus square root of scan rate ($\nu^{1/2}$) was linear (R^2=0.9938), an indication of diffusion-controlled electro-oxidative process. The current function

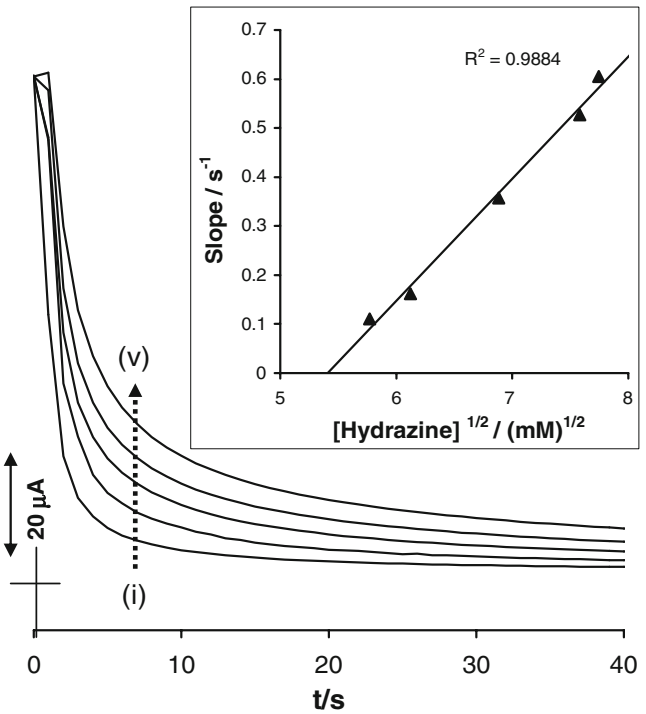

Fig. 10 Chronoamperometric evolutions of the EPPGE-SWCNT-Ni in 0.1-M Na_2SO_4 solution containing different concentrations of hydrazines (0.0, 33.3, 47.4, 50.5 and 54.5 µM (from (*i*) to (*v*)) at fixed potential of 0.6 V. *Inset* is plot of slope vs square root of the concentration of hydrazine

plot (Fig. 9b) confirms coupled chemical reaction (EC_{cat}) for hydrazine. Recall that the electro-oxidation of hydrazine in carbon-based electrodes follows a four-electron process generating nitrogen and water as products. Lin and Bocarsly [1] had elegantly described the electro-oxidation of hydrazine at nickel-ferricyanide-modified electrode, proposing series of very fast sequential charge transfer processes with intermediates that also adsorb on the electrode. From the results above, we may thus conclude here that the electro-oxidation process of hydrazine in our electrode system does not only occur at the SWCNT-metal film–solution interface; due to its small size [1], hydrazine molecule has the possibility of penetrating the SWCNT-metal film. Three main rate-limiting possibilities could be (1) mass transport of hydrazine in the solution, (2) diffusion or permeation of the hydrazine and/or its intermediates through the SWCNT-metal film and (3) charge transport through the film (or rate at which the metal catalyst is regenerated). On the basis of the information, we suggest the following general mechanism for the oxidation of hydrazine. The redox process of the SWCNT-confined metal (M = Ni or Fe or Co) species is:

$$\left(M^{3+}\right)\text{film} \rightleftharpoons \left(M^{2+}\right)\text{film} + e- \quad (1)$$

The interaction of the M^{3+} with aqueous hydrazine results to the regeneration of the M^{2+} and the formation of hydrazine oxidation intermediates:

$$\left(M^{3+}\right) + \text{Hydrazine (aq)} \rightarrow \left(M^{3+}\right)\text{film (Hydrazine)} \quad (2)$$

$$\left(M^{3+}\right)\text{film (Hydrazine)} \rightarrow \left(M^{2+}\right)\text{film} + \text{Intermediates} + e- \quad (3)$$

The oxidation intermediate(s) are further oxidized to the final product(s), via similar mediated electro-oxidation process:

$$\left(M^{3+}\right)\text{film (Intermediates)} \rightarrow \left(M^{2+}\right)\text{film} + \text{Products} \quad (4)$$

The enhanced response of the Ni^{2+}/Ni^{3+} redox process at high scan rates suggests that Fig. 9 (inset) may be ascribed to this efficient regeneration of the Ni^{2+} ions on the SWCNTs surface by hydrazine and its oxidation products.

Chronoamperometric investigations

Further studies on electro-oxidative processes of hydrazine solution at the EPPGE-SWCNT-Ni were investigated using chronoamperometric experiments. Figure 10 shows typical results obtained from chronoamperometric experiments performed by polarising the working electrode potentials at 0.60 V.

A linear relationship between background-subtracted transient current and hydrazine concentrations was obtained as:

$$\begin{aligned} I/\mu A = (0.517 \pm 0.018)[\text{hydrazine}] \\ /\mu M - (9.922 \pm 0.845)\left(R^2 = 0.9954\right) \end{aligned} \quad (5)$$

The sensitivity was calculated as 0.52±0.02 μA/μM (R^2=0.9954) while the limit of detection (LoD=3.3 *s*/*m* [85], where *s* is the relative standard deviation of the intercept and *m* the slope of the linear current versus the concentration of hydrazine) was 5.3±0.1 μM.

The catalytic rate constants (k) for the oxidation of hydrazine at both EPPGE-SWCNT-Ni and EPPGE-SWCNT-Fe were estimated from the relationship [86, 87] (Eq. 12):

$$\frac{I_{cat}}{I_{buff}} = \pi^{1/2}(kCt)^{1/2} \quad (6)$$

where I_{cat} and I_{buff} are the currents in the presence and absence of hydrazine, respectively; k is the catalytic rate constant and *t* is the time in seconds. From the plots of I_{cat}/I_{buff} vs $t^{1/2}$ at different hydrazine concentrations (not shown) and a plot of the slopes vs square root of the hydrazine concentrations (exemplified with EPPGE-SWCNT-Ni in Fig. 10 inset), k values were approximately the same, 2.2×10^4, 2.0×10^4 and 0.24×10^4 $cm^3\ mol^{-1}\ s^{-1}$ for EPPGE-SWCNT-Ni, EPPGE-SWCNT-Fe and EPPGE-SWCNT-Co, respectively, suggesting that the electrocatalytic oxidation of hydrazine was the least favoured at the EPPGE-SWCNT-Co but essentially the same for both EPPGE-SWCNT-Ni and EPPGE-SWCNT-Fe. The diffusion coefficient, *D*, of hydrazine at the EPPGE-SWCNT-Ni was estimated from the Cottrell equation [69]:

$$I = \frac{nFAD^{1/2}C}{\pi^{1/2}t^{1/2}} \quad (7)$$

where *C* is the bulk concentration (mole per cubic centimetre), *A* is the area of the electrode in square centimetre and assuming $n \approx 4$ [1, 83, 84]. From the experimental plots of *I* versus $t^{-1/2}$ at different concentrations (not shown), the diffusion coefficient *D* of hydrazine was calculated as 2.5×10^{-5} $cm^2\ s^{-1}$.

Conclusion

We have shown that edge-plane pyrolytic graphite electrodes modified with Aldrich SWCNTs electro-decorated with nickel and iron nanoparticles exhibit comparable electrochemical response in buffered aqueous solution (pH 7.0) and towards electro-oxidation of hydrazine in Na_2SO_4

solution. Also, we established from electrochemical impedance spectroscopy that these SWCNT-metal hybrids are rather complicated and follow electrical equivalent circuit model typical of adsorption-controlled charge transfer kinetics. EIS data obtained in a simple redox probe, $[Fe(CN)_6]^{3-}/([Fe(CN)_6]^{4-}$, showed that EPPGE-SWCNT and EPPGE-SWCNT-Ni followed electrical equivalent circuit models typical of partial charge transfer or adsorption-controlled kinetics with some resemblance to the behaviour of electrolyte–insulator–semiconductor sensors. These differences in the data clearly, and for the first time, provide some insights into the electro-oxidative mechanism of hydrazine at carbon electrodes modified with single-walled carbon nanotubes decorated with metal and metal oxide films.

Acknowledgements We thank the University of Pretoria and the National Research Foundation (GUN # 2073666) for their support. ASA thanks the University of Pretoria for graduate bursary and the Obafemi Awolowo University, Ile-Ife, Nigeria, for a paid study leave. We thank Chris and Andrew of the Microscopy Unit for assistance with the field emission scanning electron microscopy experiments.

References

1. Lin C, Bocarsly AB (1991) J Electroanal Chem Interfacial Electrochem 300:325–345
2. Razmi-Nerbin H, Pournaghi-Azar MH (2002) J Solid State Electrochem 6:126–133
3. Zhao Y-D, Zhang W-D, Chen H, Luo Q-M (2002) Talanta 58:529–534
4. Geraldo D, Linares C, Chen Y-Y, Ureta-Zanartu S, Zagal JH (2002) Electrochem Commun 4:182–187
5. Pournaghi-Azar MH, Sabzi R (2003) J Electroanal Chem 543:115–125
6. Yamada K, Asazawa K, Yasuda K, Loroi T, Tanaka H, Miyazaki Y, Kobayashi T (2003) J Power Sources 115:236–242
7. Linares C, Geraldo D, Paez M, Zagal JH (2003) J Solid State Electrochem 7:626–631
8. Ozoemena KI (2006) Sensors 6:874–891
9. Revenga-Parra M, Lorenzo E, Pariente F (2005) Sens Actuators B 107:678–687
10. Cardenas-Jiron GI, Paredes-Garcia V, Venegas-Yazigi D, Zagal JH, Paez M, Costamagna J (2006) J Phys Chem A 110:11870–11875
11. Jena BK, Raj CR (2007) J Phys Chem C 111:6228–6232
12. Zare HR, Nasirizadeh N (2007) Electrochim Acta 52:4153–4160
13. Majidi MR, Jouyban A, Asadpour-Zeynali K (2007) Electrochim Acta 52:6248–6253
14. Gao G, Guo D, Wang C, Li H (2007) Electrochem Commun 9:1582–1586
15. Yamada K, Yasuda K, Tanaka H, Miyazaki Y, Kobayashi T (2003) J Power Sources 122:132–137
16. Yamada K, Yasuda K, Fujiwara N, Siroma Z, Tanaka H, Miyazaki Y, Kobayashi T (2003) Electrochem Commun 5:892–896
17. Becker RA, Barrows LR, Shank RC (1981) Carcinogenesis 2:1181–1188
18. Homeland Security Information Bulletin (2003) US Department of Homeland Security, Washington DC, May
19. Wiles PG, Abrahamson J (1978) Carbon 6:341–349
20. Iijima S (1991) Nature 354:56–58
21. Britto PJ, Santhanam KSV, Ajayan PM (1996) Bioelectrochem Bioenergetics 41:121–125
22. Gooding JJ (2005) Electrochim Acta 50:3049–3060
23. Wang J (2005) Electroanalysis 17:7–14
24. Chen X, Yang Y, Ding M (2006) Anal Chim Acta 557:52–56
25. Jiang L, Wang R, Li X, Jiang L, Lu G (2005) Electrochem Commun 7:597–601
26. Zhao G-C, Zhang L, Wei X-W, Yang Z-S (2003) Electrochem Commun 5:825–829
27. Moore RR, Banks CE, Compton RG (2004) Analyst 129:755–758
28. Fei S, Chen J, Yao S, Deng G, He D, Kuang Y (2005) Anal Biochem 339:29–35
29. Hu C, Yang C, Hu S (2007) Electrochem Commun 9:128–134
30. Zhao Q, Gan Z, Zhuang Q (2002) Electroanalysis 14:1609–1613
31. Siswana MP, Ozoemena KI, Nyokong T (2006) Electrochim Acta 52:114–122
32. Ozoemena KI, Nyokong T, Nkosi D, Chambrier I, Cook MJ (2007) Electrochim Acta 52:4132–4143
33. Salimi A, Hallaj R, Soltanian S (2007) Biophys Chem 130:122–131
34. Pillay J, Ozoemena KI (2007) Electrochim Acta 52:3630–3640
35. Pillay J, Ozoemena KI (2007) Chem Phys Lett 441:72–77
36. Satishkumar BC, Vogl EM, Govindaraj A, Rao CNR (1996) J Phys D 29:3173–3176
37. Lu J (2007) Carbon 45:1599–1605
38. Ayala P, Freer FL, Gu L, Smith DJ, Solorzano IG, Macedo DW, Sande JBV, Terrones H, Rodriguez-Manzo J, Terrones M (2006) Chem Phys Lett 431:104–109
39. Tsai M-C, Yeh T-K, Tsai C-H (2006) Electrochem Commun 8:1445–1452
40. Bittencourt C, Felten A, Ghijsen J, Pireaux JJ, Drube W, Erni R, Tendeloo VG (2007) Chem Phys Lett 436:368–372
41. Tzitzios V, Georgakilas V, Oikonomou E, Karakassides M, Petridis D (2006) Carbon 44:848–853
42. Chen W, Pan X, Bao X (2007) J Am Chem Soc 129:7421–7426
43. Gao XP, Zhang Y, Chen X, Pan GL, Yan J, Wu F, Yuan HT, Song DY (2004) Carbon 42:47–52
44. Salimi A, Hallaj R, Soltanian S, Mamkhezri H (2007) Anal Chim Acta 594:24–31
45. Wildgoose GG, Banks CE, Compton RG (2006) Small 2:182–193
46. Dong B, He B-L, Huang J, Gao G-Y, Yang Z, Li H-L (2008) J Power Sources 175:266–271
47. Guo D-J, Li H-L (2005) J Colloid Interface Sci 286:274–279
48. Dai X, Wildgoose GG, Compton RG (2006) Analyst 131:1241–1247
49. Ji X, Banks CE, Holloway AF, Jurkschat K, Thorogood CA, Wildgoose GG, Compton RG (2006) Electroanalysis 18:2481–2485
50. Gao G, Guo D, Wang C, Li H (2007) Electrochem Commun 9:1582–1586
51. Duarte MME, Stefenel MM, Mayer CE (2002) J Arg Chem Soc 90:111–122
52. Zare HR, Sobhani Z, Mazloum-Ardakani M (2007) J Solid State Electrochem 11:971–979
53. Majidi MR, Jouyban A, Asadpour-Zeynali K (2007) Electrochim Acta 52:6248–6253
54. Li X, Zhang S, Sun C (2003) J Electroanal Chem 553:139–145
55. Baron R, Sljukic B, Salter C, Crossley A, Compton RG (2007) Electroanalysis 19:1062–1068
56. Casella IG, Rosa S, Desimoni E (1998) Electroanalysis 10:1005–1009
57. Banks CE, Crossley A, Salter C, Wilkins SJ, Compton RG (2006) Angew Chem Int Ed 45:2533–2537
58. Kruusma J, Mould N, Jurkschat K, Crossley A, Banks CE (2007) Electrochem Commun 9:2330–2333
59. Jones CP, Jurkschat K, Crossley A, Compton RG, Riehl BL, Banks CE (2007) Langmuir 23:9501–9504
60. Jurkschat K, Ji X, Crossley A, Compton RG, Banks CE (2007) Analyst 132:21–23
61. Pumera M (2007) Langmuir 23:6453–6458

62. Ozoemena KI, Pillay J, Nyokong T (2006) Electrochem Commun 8:1391–1396
63. Pillay J, Ozoemena KI (2007) Electrochem Commun 9:1816–1823
64. Salimi A, Sharifi E, Noorbakhsh A, Soltanian S (2006) Electrochem Commun 8:1499–1508
65. Salimi A, Sharifi E, Noorbakhsh A, Soltanian S (2007) Biophys Chem 125:540–548
66. Salimi A, Sharifi E, Noorbakhsh A, Soltanian S (2007) Biosens Bioelectron 22:3146–3153
67. Duarte MME, Pilla AS, Sieben JM, Mayer CE (2006) Electrochem Commun 8:159–164
68. Day TM, Unwin PR, Macpherson JV (2007) Nano Lett 7:51–57
69. Giovanelli D, Lawrence NS, Wilkins SJ, Jiang L, Jones TGJ, Compton RG (2003) Talanta 61:211–220
70. Bard AJ, Faulkner LR (2001) Electrochemical methods: fundamentals and applications, 2nd edn. Wiley, Hoboken
71. Ozoemena KI, Nyokong T (2005) Talanta 67:162–168
72. Peng C, Jin J, Chen GZ (2007) Electrochim Acta 53:525–537
73. Barsoukov E, Macdonald JR (2005) Impedance spectroscopy: theory, experiment, and applications, 2nd edn. Wiley, Hoboken
74. Wu X, Ma H, Chen S, Xu Z, Sui A (1999) J Electrochem Soc 146:1847–1853
75. Nurk G, Kasuk H, Lust K, Janes A, Lust E (2003) J Electroanal Chem 553:1–19
76. Hu C, Dang X, Hu S (2004) J Electroanal Chem 572:161–171
77. Thomberg T, Nerut J, Lust E (2006) J Electroanal Chem 586: 237–246
78. Monk PMS (2001) Fundamentals of electroanalytical chemistry. Wiley, Chichester, p 172
79. Bisquert J, Randriamahazaka H, Garcia-Belmonte G (2005) Electrochim Acta 51:627–640
80. Jafarian M, Mahjani MG, Heli H, Gobal F, Khajehsharifi H, Hamedi MH (2003) Electrochim Acta 48:3423–3429
81. Majdi S, Jabbari A, Heli H, Moosavi-Movahedi AA (2007) Electrochim Acta 52:4622–4629
82. Bonanos E, Steele BCH, Butler EP (2005) In: Barsoukov E, Macdonald JR (eds) Impedance spectroscopy: theory experiment, and applications, 2nd edn. Wiley, Hoboken, pp 284–288
83. Boudjahem A-G, Monteverdi S, Mercy M, Bettahar MM (2004) Langmuir 20:208–213
84. Wojcieszak R, Zielinski M, Monteverdi S, Bettahar MM (2006) J Colloid Interface Sci 299:238–248
85. Christian GD (2004) Analytical chemistry, 6th edn. Wiley, New York, p 113
86. Pournaghi-Azar MH, Sabzi R (2003) J Electroanal Chem 543:115–125
87. Manesh KM, Santosh P, Gopalan AI, Lee K-P (2006) Electroanalysis 18:894–903